ESD Behavior of MWCNT Interconnects—Part I: Observations and Insights

Abhishek Mishra, *Student Member, IEEE*, Harald Gossner, *Senior Member, IEEE*, and Mayank Shrivastava, *Senior Member, IEEE*

(Invited Paper)

***Abstract*—Multiwall carbon nanotube (MWCNT)-based interconnects have been shown to outperform conventional metal interconnects. For reliable operation of such interconnects, it is imperative to evaluate their reliability at possible fatal events. Here, we report the ESD reliability of MWCNT-based interconnects. High failure current of ∼10 mA and unique failure behavior involving discrete and gradual breakdown of individual shells is reported. It was found that MWCNT interconnects change resistance in steps of fundamental quantum resistance ($h/2e^2$) after individual shell burning. The role of individual shells, diameter, and resistance of the tube in deciding the ESD behavior is investigated, while monitoring the response on a shell-by-shell basis. Contrary to widespread notion of immunity of MWCNT interconnects to electromigration, the ESD-induced melting of contacts is also observed.**

***Index Terms*—MWCNT, interconnects, ESD, reliability.**

I. Introduction

AGGRESSIVE downscaling of transistors and interconnects coupled with increase in power consumption has lead to the occurrence of extremely high power densities and formation of hot-spots across the semiconductor integrated circuit. The consequent high temperatures generally result in catastrophic failure of interconnects [1]. Such failure issues are addressed by reducing the performance of the integrated circuit [2]. In such a scenario, the interconnects are set to play a vital role in deciding performance and reliability trade-off. In conventional metal interconnects, barrier layer effect, grain boundary scattering and surface scattering increases with down-scaling [3], which in turn reduces their current carrying capacity. Moreover increase in power density makes them prone to catastrophic events like electro-migration [4], [5]. Hence there is a need to replace conventional metal interconnects with relatively more robust material. In this regard, multiwall carbon nanotubes have emerged as a promising material for future interconnects [6]–[8].

The unique band-structure of MWCNTs offer very high current carrying capacities [9], while its sp^2 hybridized carbon lattice provides extremely high mechanical strength and high thermal conductivity [10]. These properties together enable high current conduction through MWCNTs, while making them relatively more resilient to high-field and temperature induced breakdown like electro-migration. Various matured synthesis and process technologies exist for fabricating MWCNTs based interconnects. Few prominent methods include CVD based growth of MWCNT vias [11], low-pressure chemical vapor deposition (LPCVD) based aligned growth on quartz substrate [12], deterministic placement through dielectrophoresis [13], [14], deposition of long horizontal CNT bundles [15]. Device and circuit models have also been discussed and reported in the past [16], [17]. Moreover, physics of carrier transport under low and high electric fields, quantum conductance, and thermal failure in CNTs have been extensively studied for quasi-static operation [18], [19]. However, MWCNTs have still not been challenged in terms of their reliability. In order to guarantee reliable operation of MWCNTs based interconnects, it is imperative to investigate and improve their operational reliability. The long-term reliability of MWCNTs has been investigated in the past, with current densities of $10^9 A/cm^2$ reportedly recorded for duration of two weeks at the temperature of 250°C [20]. Note that the current density in the unit of Ampere per unit cross-sectional area includes the contribution of both inner and outer shells. Unfortunately, comprehensive investigations on short term reliability, especially under ESD conditions, is still not available, except for few pioneering works [21]–[24]. ESD investigations of MWCNT interconnects is vital to overall design targets, as they are set while considering the limitations of the semiconductor devices [25]. Interconnects are expected to give robust performance while carrying vital signals and power across the integrated circuit. In this contribution, we present a comprehensive investigation on ESD reliability of MWCNT interconnects, while considering two different device architectures - 1) suspended single MWCNT and 2) bundle of dielectric-supported MWCNTs. Since the performance of a MWCNT interconnect depends largely on diameter, for the overall understanding of the ESD behavior, it is instructive

Manuscript received May 17, 2017; revised August 16, 2017; accepted September 21, 2017. Date of publication September 26, 2017; date of current version December 7, 2017. This work was supported by the Department of Science and Technology, Government of India under Project SB/S3/EECE/063/2014. *(Corresponding author: Abhishek Mishra.)*

A. Mishra is with the Department of Electronic Systems Engineering, Indian Institute of Science, Bengaluru 560012, India, and also with the Center for Nanoscience and Engineering, Indian Institute of Science, Bengaluru 560012, India (e-mail: mishra@iisc.ac.in).

H. Gossner is with Intel Deutschland GmbH, 85579 Neubiberg, Germany.

M. Shrivastava is with the Department of Electronic Systems Engineering, Indian Institute of Science, Bengaluru 560012, India (e-mail: mayank@iisc.ac.in).

Color versions of one or more of the figures in this paper are available online at http://ieeexplore.ieee.org.

Digital Object Identifier 10.1109/TDMR.2017.2756924

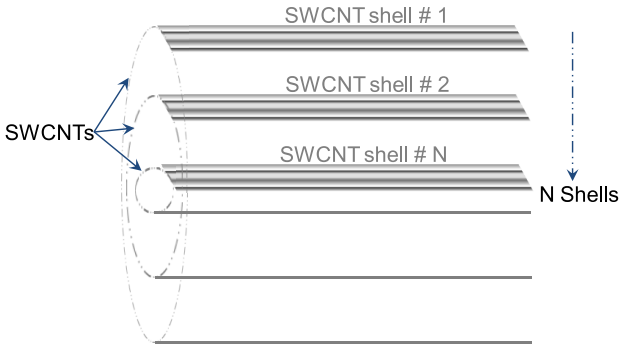

Fig. 1. Concentric cylindrical structure of multiple SWCNTs, which forms MWCNT. The inter-shell spacing is around 3.4 Å, which in turn increases with decrease in diameter of the shell [29].

to investigate MWCNTs of different diameters. Interestingly, different kinds of interconnects require different architectures of MWCNTs. For example, individual MWCNTs can act as on-chip interconnects, while the same tubes in bundled architecture can deliver huge power by acting as through-silicon via. Rest of the paper is arranged as follows - Section II gives a brief overview of MWCNTs, Section III describes the experimental details, Section IV discusses breakdown characteristics, Section V presents the analysis of ESD-induced failure, Section VI discusses the possibilities of ESD-induced current annealing of the interconnect, Section VII concludes the overall work and findings.

II. Carbon Nanotubes

MWCNTs are concentric shells (figure 1) of single layer of sp^2 hybridized carbon atoms [26]. The individual shells can independently be metallic or semiconducting. The metallic tubes have zero bandgap and offers very high mobility due to linear dispersion relation. The bandgap of the semiconducting shells is given by $0.7/d\ eV$, where d is diameter of the shell in nanometers [27]. Due to this inverse dependence on diameter, the semiconducting shells with diameter more than 30 nm behave as semi-metals at room temperature. The optical phonon modes of the shells lie at relatively higher energy of 160 meV [28], which allows large mean free paths and unimpeded flow of carriers. The individual tubes can be bundled together to achieve even higher current densities. The individual shells of MWCNTs can independently be chiral, armchair or zigzag. Each configuration results in different electronic properties. The shells can be conceptually formed by wrapping of monolayer graphene. Figure 2 depicts wrapping of graphene monolayer to form CNTs. The shaded regions (figure 2i and 2ii) show the wrapping plane and portion of graphene monolayer which forms the tube. CNTs electrical properties depend on the chiral vector C_h, where: $C_h = na_1 + ma_2 = (n, m)$, ($n$, m are positive integers and $0 \leq m \leq n$); diameter (d) of the tube, which is derived from the chiral vector $|C_h| : d = \sqrt{C_h \times C_h/\pi}$ and angle ϕ ($\cos\phi = C_h \times a_1/|C_h||a_1|$), which is the angle between chiral vector and lattice vector a_1. Zigzag tubes have $\phi = 30°$ (figure 2i) and armchair tubes have $\phi = 0°$ (figure 2ii), whereas chiral tubes have $0 < \phi < 30°$. A CNT is metallic if

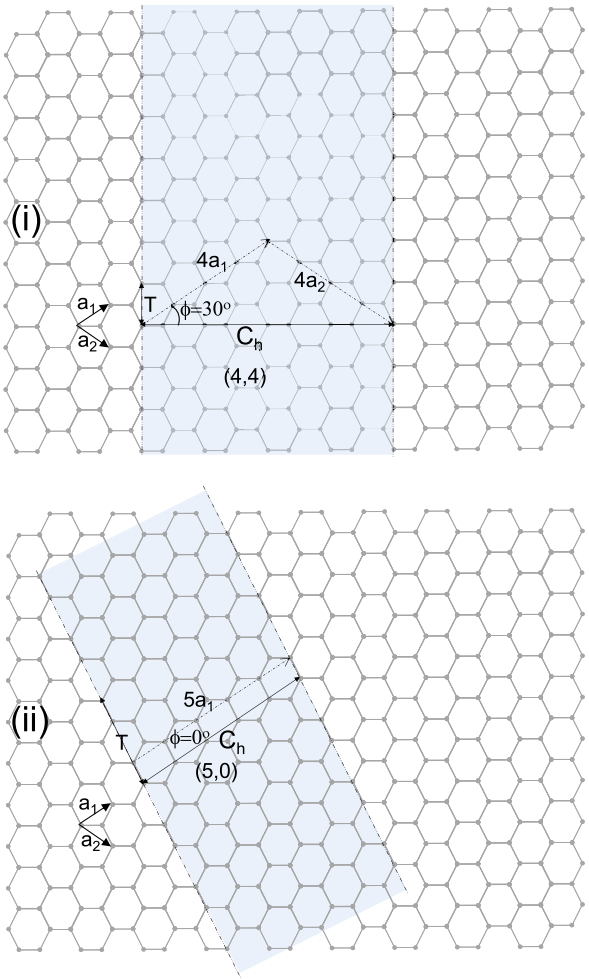

Fig. 2. Wrapping of graphene monolayer to form an (i) armchair SWCNT and (ii) zigzag SWCNT. Nanotubes in armchair configuration are metallic, while in zigzag configuration the tube can be either metallic or semiconducting.

(n m) is an integer multiple of 3 or 0, otherwise it is semiconducting [27]. Typically SWCNTs diameter ranges from 0.5 nm to 5 nm. MWCNTs can have diameter up to 100 nm. The minimum spacing between individual SWCNTs in a MWCNT is 3.4 Å. Typically MWCNT have $2/3^{rd}$ metallic SWCNTs and $1/3^{rd}$ semiconducting SWCNTs. Therefore, in general, MWCNTs are metallic in nature. Another interesting property of CNTs is related to its band structure. CNTs have multiple sub-bands at higher energies (number of sub-bands increases with CNTs diameter [30]). Moreover, CNTs have symmetric band structure, especially at low energies, i.e., high electron-hole symmetry at low energies. Figure 3a and 3b depict the band bending in metallic and semiconducting CNTs respectively. Both figure 3a and 3b show the high energy sub-bands and electron-hole symmetry. Figure 3a shows zero bandgap, whereas figure 3b shows a finite bandgap (E_g). In this work MWCNTs are used for ESD exploration.

III. Device Under Test and Measurement Setup

MWCNTs for ESD investigations were grown by thermal chemical vapour deposition (CVD) of a mixture of ferrocene and toluene at a temperature of 850 °C. For fabricating devices

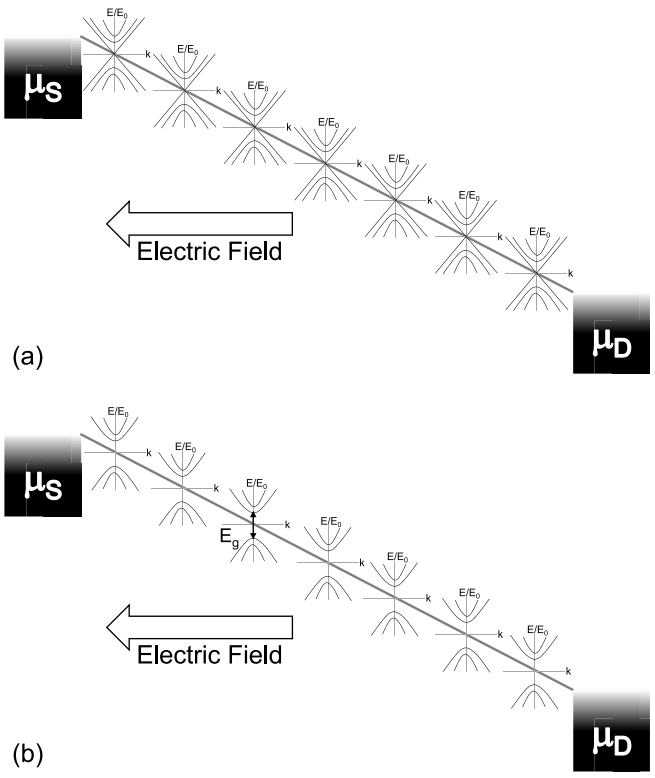

Fig. 3. Band bending in metallic (a) and semiconducting CNTs (b) depicting high energy sub-bands, electron-hole symmetry and respective bandgap, which in turn decreases with increase in diameter.

with suspended MWCNTs, the grown tubes were detached from the substrate and then dispersed individually on top of 250 nm thick Cr/Au contact pads. Cr/Au contact pads were deposited and patterned over a Si/SiO_2 substrate (thermally grown SiO_2 over a Si substrate). Spacing between individual metal pads was 2 μm (figure 4). Such a deposition technique ensured that only the outermost shell (henceforth, referred as the 1^{st} shell and its breakdown as 1^{st} breakdown) contacts the metal pads, and hence paved the way to look into the effect of ESD stress on individual shells. Devices with bundle of MWCNTs were fabricated by dielectrophoresis of MWCNT suspension across the pair of pre-patterned electrodes [13]. ESD behavior was investigated through a TLP setup shown in figure 4. It is also important to mention that this work targets fundamental behavior of MWCNTs under ESD conditions, therefore TLP pulses with different pulse widths were used for investigations, rather than emulating ESD stress using models like HBM, CDM etc. It is too early to study, for example, HBM behavior of a single MWCNT. This approach also gives physical insights into the transport behavior of CNTs under ESD conditions, which gives a vital piece of information, as the MWCNTs attain thermal equilibrium in few tens of nano-seconds.

IV. TLP I-V Characteristics

Figure 5 shows TLP I-V characteristics of 6 different MWCNT samples stressed using 100 ns, 5 ns and 10 ns TLP pulses, respectively. After each stress/TLP pulse, tubes

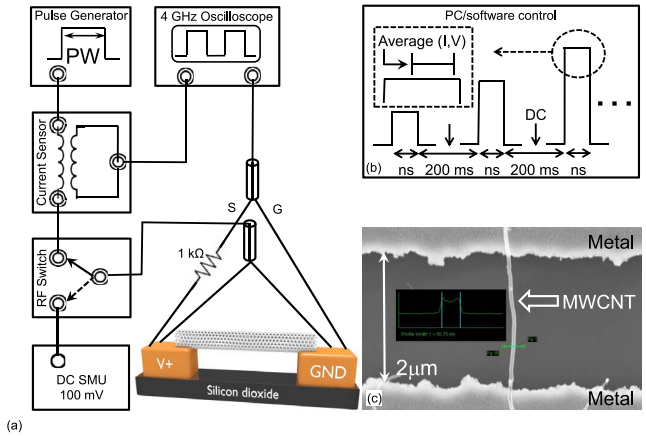

Fig. 4. (a) A 4-probe, transmission line pulsing setup, with an inductive current-sensor (5 mV/mA) and a 4 GHz sampling oscilloscope (25 GS/sec) (b) Measurement and extraction routine followed for emulation of ESD stress. (c) SEM image of one of the pristine MWCNT suspended across metal electrodes.

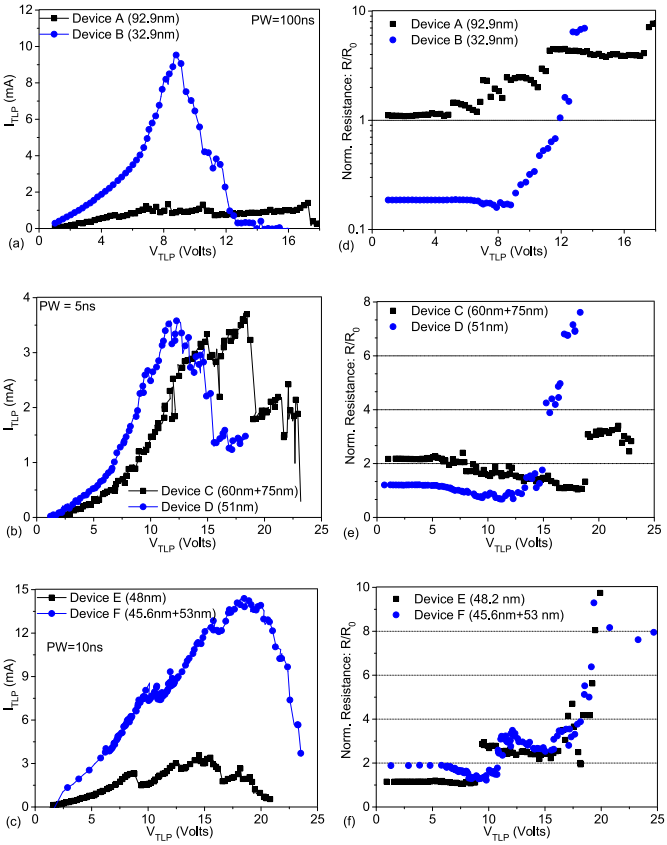

Fig. 5. (a,b,c) TLP I-V characteristics of various metallic CNT samples stressed under 100 ns, 5 ns and 10 ns TLP stress. (d,e,f) CNT tubes resistance at low-bias, extracted after each stress pulse during TLP test, in the units of fundamental quantum resistance R_0 ($= \frac{h}{2e^2}$).

resistance was extracted in the units of fundamental quantum resistance (R_0),

$$R_0 = \left(\frac{h}{2e^2}\right) \tag{1}$$

where h is Planck's constant and e is electron charge [31]. Figure 5 shows that CNTs under ESD test have pre-fail

resistances in a range of $0.1R_0$ to $2R_0$ with a distinct TLP I-V relationship at high currents. A clear metallic (linear I-V) behavior can be seen from various TLP I-V plots at lower voltages; however, MWCNT changes its behavior at high currents and fields. For example, *device A* under 100 ns TLP stress shows a liner relation till the first fail, however, *device B* shows an exponential relation after 4 V (see figure 5a). Exponential I-V relation at higher voltages can be attributed to band-to-band tunneling between non-crossing energy bands [32]. Interestingly, *device A* has a quantized (step like, in multiples of R_0) increase in tubes resistance after each fail, however *device B* shows a gradual increase in tubes resistance (see figure 5d). Other clear difference can be observed in terms of current handling capacity of *device B*. Despite of $\sim 3\times$ smaller diameter, *device B* can carry $\sim 10\times$ more current than *device A*. A similar I-V behavior can be observed from other samples *device C*, *device D* (figure 5b) and *device E*, *device F* (figure 5c) stressed under 5 ns and 10 ns TLP. *Device D* and *device C* show initially a linear I-V relation, which changes to exponential relationship at higher TLP voltages. Moreover, both the samples (with tubes resistance $> R_0$) show a step like drop in current and quantized increase in resistance after each fail. Exponential I-V relation at higher bias can also be attributed to filling of high energy states in these materials. For clarity and statistical justification of arguments presented above, few more samples (*device G*, *device H* and *device I*) were stressed using TLP (pulse widths = 20 ns, 50 ns and 500 ns, respectively). Their respective TLP I-V behaviors are depicted in figure 6, which adds to the explanations given above. In general, all the samples under test conduct at all TLP voltages, and undergo into the failure mode at higher voltages. Unlike to metals in which ESD/TLP current drops immediately after the (first) fail, MWCNTs show a gradual or step like drop in current [19], [33]. Moreover, after each failure tubes resistance either changes gradually or in steps of fundamental quantum resistance ($R_0 = h/2e^2$). This behavior can be linked with the geometry or tubes arrangement in MWCNTs (discussed in the next section). A comparison of failure current (It2, at first fail) of different samples (*device D*, *device E* and *device A*) with comparable tubes resistances ($\sim R_0$, at low-bias) and stressed under different TLP pulse widths (5 ns, 10 ns and 100 ns respectively) show a power law like relation (here $It2 \sim t^{-n}$, where $n < 0.2$), i.e., It2 falls with increasing pulse width (3.4 mA, 2.3 mA and 1.1 mA respectively). Similarly, tubes (*device B* and *device I*) with resistance $< R_0 (\sim 0.2R_0)$ show a power like behavior. Its worth highlighting that comparison of It2 must be done for tubes with comparable resistance (extracted at low-bias). Unfortunately, a comparison in terms of It2 per unit diameter is not possible given that each tube may have different number of shells available for current conduction, which is attributed to immaturity of the state-of-the-art CNT growth process available.

With the understanding of ESD behavior of suspended thick MWCNTs (diameter > 30 nm), we investigate the ESD behavior of dielectric-supported bundle of thin MWCNTs (diameter < 10 nm) in figure 6(d). Such bundle of tubes emulates the behavior of MWCNT based through-hole via [34]. The device shows step-by-step breakdown in response to high

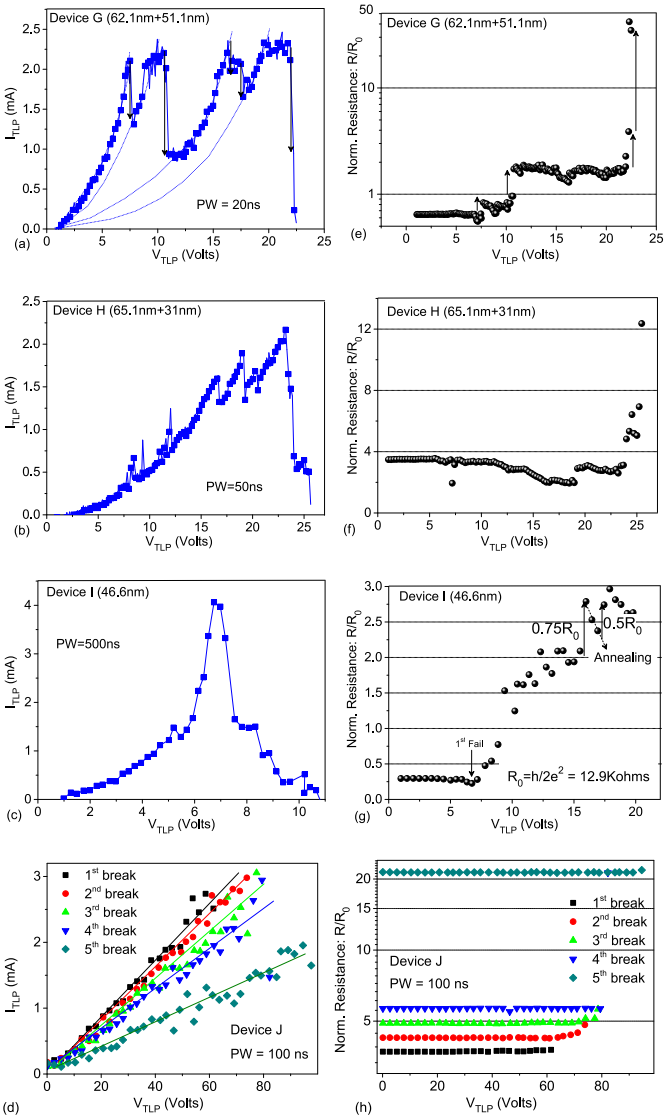

Fig. 6. (a,b,c) TLP I-V characteristics of various metallic CNT samples stressed under 20 ns, 50 ns and 500 ns TLP stress. (e,f,g) CNT tubes resistance at low-bias, extracted after each stress pulse during TLP test, in the units of fundamental quantum resistance. (d,h) Measured TLP I-V and low-bias DC characteristics of bundle of thin dielectric-supported MWCNTs. The device shows linear TLP I-V characteristics. The gradual and discrete failure is also clearly visible, where the low-bias resistance shows discrete increment situated near hundreds of kilo-ohms.

voltage ESD pulse, which is similar to the devices discussed previously. A distinct difference can be observed at high voltages. The thicker tubes show quasi-exponential behavior at high voltages, while the tubes with smaller diameter retains their linear behavior at higher voltages. This also suggests that as the outer-shells are sequentially broken by ESD pulses, the TLP I-V behavior should gradually change from quasi-exponential to linear due to reduction in number of sub-bands with decrease in diameter [30], [32].

A comparison between tube's resistance with R_0 and TLP I-V characteristics (figure 5 and 6) shows a correlation between the resistance and nature of the TLP I-V characteristics. Most of the tubes with resistance $< R_0$ give rise to an exponential increase in current at higher TLP voltages, moreover, such tubes fail with a gradual drop in current.

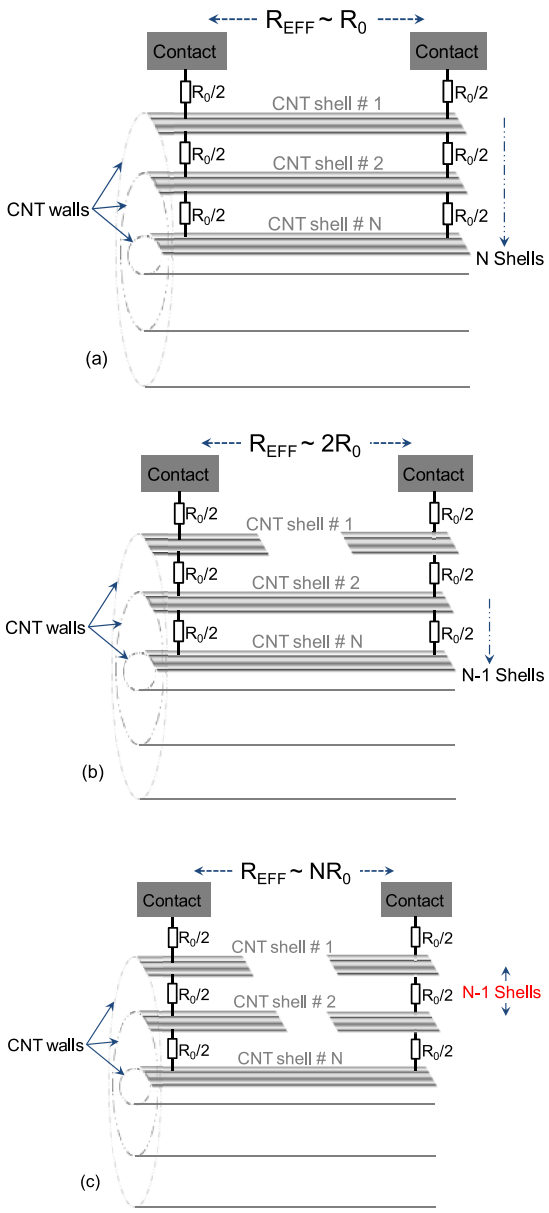

Fig. 7. A model depicting a possible way of coupling between metal pads and CNT shells and explaining step change in resistance after each fail. (a) Figure shows a possible way of CNT shell to contact coupling of a virgin device. (b-c) Show how a quantized change in tubes resistance is possible after 1^{st} and $(N\text{-}1)^{th}$ fail. (A 3D illustration of shell burning is also given in figure 10b).

On the other hand, tubes with resistance $> R_0$ mostly show a linear I-V relation till the first failure (burning of outer shell) and current drops in steps with the failure/burning of each shell. Moreover, the linearity in TLP I-V characteristics increases with decrease in diameter. This further suggests that tube's resistance increases with decrease in diameter. As discussed earlier, the quasi-exponential behavior arises because of participation of more sub-bands and inter-shell tunneling at higher voltages. Number of sub-bands in a shell increases with diameter of the shell. Moreover, the inter-shell spacing increases with reduction in diameter [29]. Due to decrease in number of sub-bands and number of shells with diameter and increase in inter-shell tunneling distance, the tubes with smaller diameter show linear behavior at high ESD voltages,

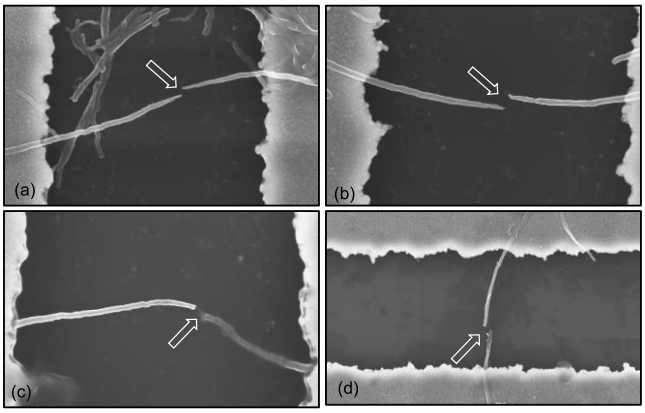

Fig. 8. Post-failure SEM images of MWCNTs damaged after ESD stress. Damage location (indicated by arrow) was often found to be at the center along the length of the tube.

while the ESD behavior of thicker tubes shifts from linear to quasi-exponential at higher TLP voltages.

Note that the failure behavior of MWCNT bundles is very different from that of a single tube. Moreover, the failure behaviour changes with variation in diameter of the tube. This is contrary to what is generally observed in conventional silicon devices or metals, where the linear scaling can relate the physical quantities among up-scaled or down-scaled devices. Although bundling of tubes and increasing the diameter, increases their current carrying capabilities, a direct linear extrapolation of the physical quantities and failure mechanism cannot be derived because of the following constraints: (i) number of CNTs in a bundle cannot be precisely controlled with the existing deposition techniques, (ii) current flowing through individual tubes is not the same and depends on various factors like chirality, defect density, and contact resistance, which cannot be directly controlled via the available set of experimental methods. (iii) electrical properties of single nanotube are entirely different from that of the bundle. For example, single MWCNT can behave as a ballistic conductor; however the same when bundled behaves like a diffusive conductor. (iv) Both inter-shell spacing and number of sub-bands show strong dependence on diameter of shells/tube.

V. Failure Analysis

In this section ESD failure behavior of CNT samples is discussed. However, before explaining failure behavior, we have tried to develop a generalized model for the quantized change in resistance after each fail (seen as a fall in I-V characteristics). Figure 7a shows a possible way of contacting (coupling) between CNT shells and metal pads. MWCNTs have multiple concentric shells (also depicted in figure 10b). The model shows N groups of CNT shells, each group consists of one or more CNT shells. Figure 7b and 7c show two extreme cases after failure and respective effective tubes resistance, depicting the quantized change in resistance. Its worth pointing that increase of tubes resistance does not result from degrading contacts. It is due to removal of single carbon layers, which is a novel failure mechanism. This is proven by the location of the final fail in the center of the CNT tube as shown in

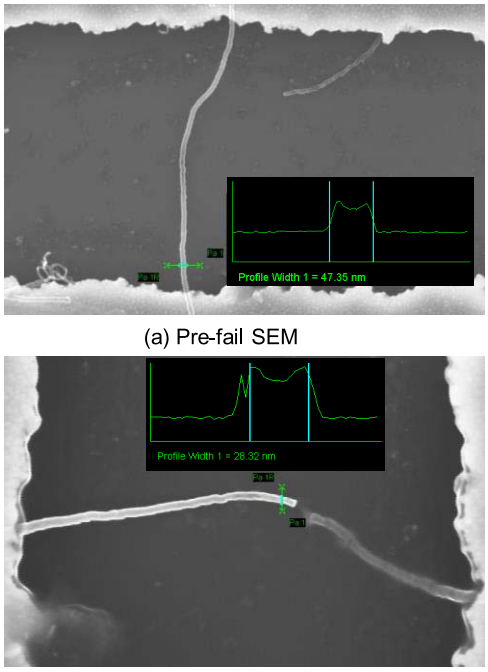

Fig. 9. Thinning of carbon nanotube close to the failure point validating loss of carbon material under ESD stress. (a) SEM image of virgin device with tubes diameter of 47.35 nm. (b) SEM image of damaged tube with reduced diameter (28.32 nm) close to the failure point.

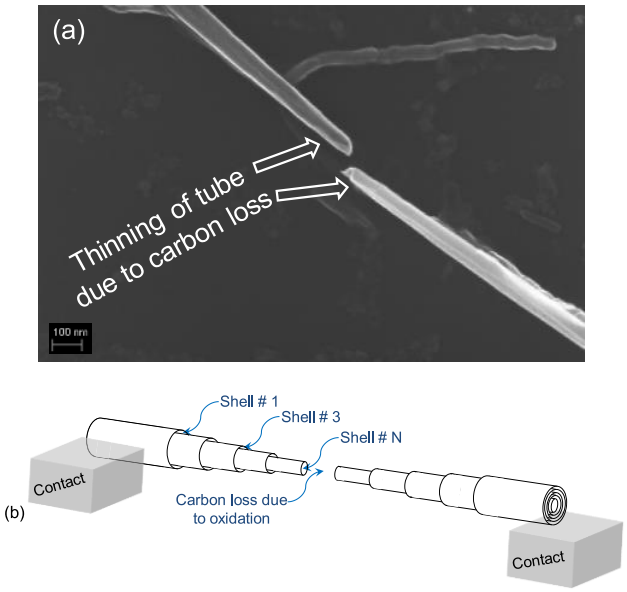

Fig. 10. (a) A closer view of failure location in one of the MWCNT sample, clearly depicting reduced tubes diameter and loss of carbon next to failure point. (b) A pictorial representation of the same.

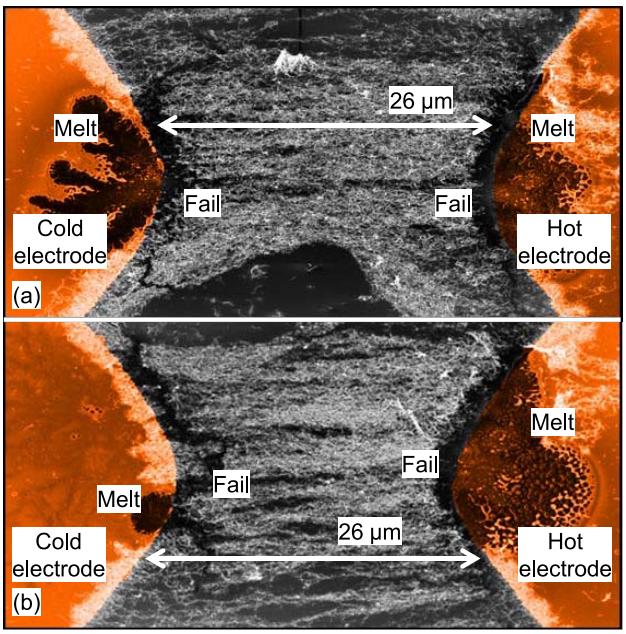

Fig. 11. (a,b) Post-breakdown SEM images of bundle of thin MWCNTs. Failure of individual tubes and melting of metal electrodes are clearly visible near both hot and cold electrodes. Melting of the electrodes show transfer of huge amount of thermal energy to contacts via MWCNT channels.

SEM images (figure 8). The SEM images in figure 8 further shows: (i) damage location at the center position, which can be attributed to thermal failure of diffusive CNTs, and (ii) no carbon left over at the failure site, i.e., carbon materials have no molten state. Failure at the center (i) can be explained using diffusive carrier transport, in which carrier travelling from one terminal to the other uniformly loses its energy across the channel (here CNT). As the center of tube will see highest thermal resistance, this region will gain the maximum heat (location of hot spot) and therefore will burn first. Later (ii) can be explained as loss of carbon due to oxidation under extreme stress (thermal) conditions. This is also evident from figure 9 and 10, both of which show thinning of carbon nanotube close to the damage site.

The failure behavior of bundle of thin MWCNTs is distinctively different from individual thick MWCNT. Electromigration of contact metal is observed in devices with bundle of thin MWCNTs (figure 11). Interestingly, ESD-induced melting of metal can be noticed at both hot and cold electrodes. This shows that under ESD conditions, MWCNTs, due to high thermal conductivity, transfers a huge amount of thermal energy to metal contacts. Melting of metal contacts is not observed in case of thick tubes, even though they carry relatively more ESD current. This can be attributed to reduction in axial thermal conductivity, which decreases with increase in diameter [35].

VI. ESD-Induced Current Annealing

In this section we investigate the pre-breakdown behaviour of MWCNTs under ESD conditions. Figure 12 shows the TLP IV characteristics and resistance of MWCNTs, where the latter shows permanent decrease in pre-breakdown region. Such a decrease in resistance indicates ESD-induced annealing of the MWCNT and can be explained by considering ESD-assisted thermal transport through the MWCNT. Under ESD conditions, a huge amount of thermal energy flows through quasi-1D constricted channel of MWCNTs, which can cause oxidation of carbon material. Steady-state oxidation of carbon material happens at the temperature of around 700°C. The Arrhenius relation predicts an exponential dependence of

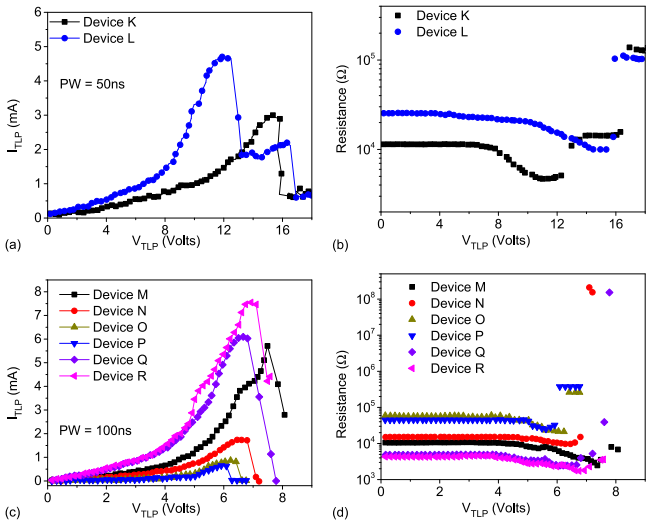

Fig. 12. (a,b) TLP I-V characteristics and corresponding change in device resistance of dielectric-supported (a,b) and suspended (c,d) MWCNTs. The suspended tubes show enhanced effect of annealing and relatively more increase in current than the dielectric-supported tubes.

rate of oxidation of carbon on temperature [36], consequently under ESD conditions, which involves application of high-voltage nano-second time scale pulses, the carbon material can sustain much higher temperatures, without showing any significant breakdown or oxidation of outer-shells [21]. Although existence of high local temperature for few nano-seconds can cause negligible or slow rate of oxidation of MWCNTs, it can result in appreciable desorption of adsorbents from the surface of MWCNTs and metal-MWCNT interface. Moreover, it can also result in diffusion of metal atoms into the MWCNT. Desorption from channel results in reduction in scattering centers, while desorption from MWCNT-metal interface brings reduction in distance along which carriers tunnel across the interface, thereby increasing the interaction between p_z orbital of outer-shell of MWCNT and d orbital of metal. ESD current in both the cases show substantial increase due to annealing of channel and contacts respectively. Such a current annealing is captured in figure 12, where the device resistance shows permanent decrease after sustaining high-bias TLP pulses. The current annealing is expected to be more pronounced in suspended semi-ballistic tubes than diffusive dielectric-supported tubes, as the surface phonon modes of substrate in latter case can remove heat from MWCNT. This is evident in figure 12, where the suspended tubes show enhanced increment in current than the dielectric-supported tubes. Similarly, the high-bias short duration pulses are expected to cause current annealing before initiating oxidation of the tube, while relatively low-bias long pulses are expected to initiate gradual oxidation of shell without causing any current annealing of the tube.

VII. Conclusion

In summary, we have investigated the ESD failure behavior of MWCNT interconnects, while considering two different device architectures - suspended single MWCNTs and bundle of dielectric-supported MWCNTs. The ESD behavior of MWCNT interconnects was found to be different from metals, featuring step-by-step destruction of individual shells with increasing pulse amplitude. Moreover, a quantized increase in tube's resistance in the units of $h/2e^2$ was observed. The quantized increase in tube's resistance is used to model a possible scheme for CNT-to-metal contact. At high ESD current, annealing and electromigration of contacts was observed in many devices, which emphasizes the need for robust metal contacts for reliable operation of MWCNT interconnects.

Acknowledgment

The authors acknowledge Prof. Srinivasan Raghavan (CeNSE, IISc) for fruitful discussions.

References

[1] K. Banerjee and A. Mehrotra, "Global (interconnect) warming," *IEEE Circuits Devices Mag.*, vol. 17, no. 5, pp. 16–32, Sep. 2001.

[2] M. Shafique, S. Garg, T. Mitra, S. Parameswaran, and J. Henkel, "Dark silicon as a challenge for hardware/software co-design: Invited special session paper," in *Proc. Int. Conf. Hardw./Softw. Codesign Syst. Synthesis*, 2014, pp. 1–10. [Online]. Available: http://doi.acm.org/10.1145/2656075.2661645

[3] S. Im, N. Srivastava, K. Banerjee, and K. E. Goodson, "Scaling analysis of multilevel interconnect temperatures for high-performance ICs," *IEEE Trans. Electron Devices*, vol. 52, no. 12, pp. 2710–2719, Dec. 2005.

[4] C.-K. Hu, R. Rosenberg, H. S. Rathore, D. B. Nguyen, and B. Agarwala, "Scaling effect on electromigration in on-chip Cu wiring," in *Proc. IEEE Int. Interconnect Technol. Conf.*, San Francisco, CA, USA, 1999, pp. 267–269.

[5] J. Lienig, "Interconnect and current density stress: An introduction to electromigration-aware design," in *Proc. Int. Workshop Syst. Level Interconnect Prediction*, San Francisco, CA, USA, 2005, pp. 81–88. [Online]. Available: http://doi.acm.org/10.1145/1053355.1053374

[6] G. F. Close, S. Yasuda, B. Paul, S. Fujita, and H.-S. P. Wong, "A 1 GHz integrated circuit with carbon nanotube interconnects and silicon transistors," *Nano Lett.*, vol. 8, no. 2, pp. 706–709, 2008, doi: 10.1021/nl0730965.

[7] H. Li, C. Xu, N. Srivastava, and K. Banerjee, "Carbon nanomaterials for next-generation interconnects and passives: Physics, status, and prospects," *IEEE Trans. Electron Devices*, vol. 56, no. 9, pp. 1799–1821, Sep. 2009.

[8] N. Srivastava, H. Li, F. Kreupl, and K. Banerjee, "On the applicability of single-walled carbon nanotubes as VLSI interconnects," *IEEE Trans. Nanotechnol.*, vol. 8, no. 4, pp. 542–559, Jul. 2009.

[9] H. J. Li, W. G. Lu, J. J. Li, X. D. Bai, and C. Z. Gu, "Multichannel ballistic transport in multiwall carbon nanotubes," *Phys. Rev. Lett.*, vol. 95, Aug. 2005, Art. no. 086601. [Online]. Available: https://link.aps.org/doi/10.1103/PhysRevLett.95.086601

[10] A. A. Balandin, "Thermal properties of graphene and nanostructured carbon materials," *Nat. Mater.*, vol. 10, no. 8, pp. 569–581, Jul. 2011, doi: 10.1038/nmat3064.

[11] T. Wang *et al.*, "Through-silicon vias filled with densified and transferred carbon nanotube forests," *IEEE Electron Device Lett.*, vol. 33, no. 3, pp. 420–422, Mar. 2012.

[12] N. Patil *et al.*, "Wafer-scale growth and transfer of aligned single-walled carbon nanotubes," *IEEE Trans. Nanotechnol.*, vol. 8, no. 4, pp. 498–504, Jul. 2009.

[13] A. H. Monica, S. J. Papadakis, R. Osiander, and M. Paranjape, "Wafer-level assembly of carbon nanotube networks using dielectrophoresis," *Nanotechnology*, vol. 19, no. 8, 2008, Art. no. 085303. [Online]. Available: http://stacks.iop.org/0957-4484/19/i=8/a=085303

[14] G. F. Close and H.-S. P. Wong, "Fabrication and characterization of carbon nanotube interconnects," in *Proc. IEEE Int. Electron Devices Meeting*, Washington, DC, USA, Dec. 2007, pp. 203–206.

[15] H. Li, W. Liu, A. M. Cassell, F. Kreupl, and K. Banerjee, "Low-resistivity long-length horizontal carbon nanotube bundles for interconnect applications—Part I: Process development," *IEEE Trans. Electron Devices*, vol. 60, no. 9, pp. 2862–2869, Sep. 2013.

[16] A. Nieuwoudt and Y. Massoud, "RC circuit model for multi-walled carbon nanotubes," in *Proc. 7th IEEE Conf. Nanotechnol.*, Hong Kong, Aug. 2007, pp. 660–663.

[17] H. Li, W.-Y. Yin, K. Banerjee, and J.-F. Mao, "Circuit modeling and performance analysis of multi-walled carbon nanotube interconnects," *IEEE Trans. Electron Devices*, vol. 55, no. 6, pp. 1328–1337, Jun. 2008.
[18] A. Urbina, I. Echeverria, A. Pérez-Garrido, A. Diaz-Sánchez, and J. Abellán, "Quantum conductance steps in solutions of multiwalled carbon nanotubes," *Phys. Rev. Lett.*, vol. 90, no. 10, Mar. 2003, Art. no. 106603. [Online]. Available: https://link.aps.org/doi/10.1103/PhysRevLett.90.106603
[19] P. G. Collins, M. Hersam, M. Arnold, R. Martel, and P. Avouris, "Current saturation and electrical breakdown in multiwalled carbon nanotubes," *Phys. Rev. Lett.*, vol. 86, no. 14, pp. 3128–3131, Apr. 2001. [Online]. Available: http://link.aps.org/doi/10.1103/PhysRevLett.86.3128
[20] B. Q. Wei, R. Vajtai, and P. M. Ajayan, "Reliability and current carrying capacity of carbon nanotubes," *Appl. Phys. Lett.*, vol. 79, no. 8, pp. 1172–1174, 2001, doi: 10.1063/1.1396632.
[21] M. Shrivastava, N. Kulshrestha, and H. Gossner, "ESD investigations of multiwalled carbon nanotubes," *IEEE Trans. Device Mater. Rel.*, vol. 14, no. 1, pp. 555–563, Mar. 2014.
[22] M. Shrivastava and H. Gossner, "ESD behavior of metallic carbon nanotubes," in *Proc. Elect. Overstress/Electrostat Discharge Symp.*, Tucson, AZ, USA, Sep. 2014, pp. 1–6.
[23] A. Mishra and M. Shrivastava, "New insights on the ESD behavior and failure mechanism of multi wall CNTs," in *Proc. IEEE Int. Rel. Phys. Symp.*, Pasadena, CA, USA, Apr. 2016, pp. EL-8-1–EL-8-5.
[24] A. Mishra and M. Shrivastava, "Unique current conduction mechanism through multi wall CNT interconnects under ESD conditions," in *Proc. 38th Elect. Overstress/Electrostatic Discharge Symp.*, Garden Grove, CA, USA, Sep. 2016, pp. 1–6.
[25] T. Smedes and Y. Li, "ESD phenomena in interconnect structures," in *Proc. Elect. Overstress/Electrostatic Discharge Symp.*, Las Vegas, NV, USA, Sep. 2003, pp. 1–8.
[26] S. Iijima, "Helical microtubules of graphitic carbon," *Nature*, vol. 354, no. 6348, pp. 56–58, Nov. 1991, doi: 10.1038/354056a0.
[27] H. Wong and D. Akinwande, *Carbon Nanotube and Graphene Device Physics*. Cambridge, U.K.: Cambridge Univ. Press, 2010.
[28] J.-Y. Park *et al.*, "Electron phonon scattering in metallic single-walled carbon nanotubes," *Nano Lett.*, vol. 4, no. 3, pp. 517–520, 2004, doi: 10.1021/nl035258c.
[29] C.-H. Kiang, M. Endo, P. M. Ajayan, G. Dresselhaus, and M. S. Dresselhaus, "Size effects in carbon nanotubes," *Phys. Rev. Lett.*, vol. 81, pp. 1869–1872, Aug. 1998. [Online]. Available: https://link.aps.org/ doi/10.1103/PhysRevLett.81.1869
[30] A. Naeemi and J. D. Meindl, "Compact physical models for multiwall carbon-nanotube interconnects," *IEEE Electron Device Lett.*, vol. 27, no. 5, pp. 338–340, May 2006.
[31] S. Datta, *Electronic Transport in Mesoscopic Systems* (Cambridge Studies in Semiconductor Physics). Cambridge, U.K.: Cambridge Univ. Press, 1997.
[32] A. Svizhenko, M. P. Anantram, and T. R. Govindan, "Ballistic transport and electrostatics in metallic carbon nanotubes," *IEEE Trans. Nanotechnol.*, vol. 4, no. 5, pp. 557–562, Sep. 2005.
[33] J. Y. Huang *et al.*, "Atomic-scale imaging of wall-by-wall breakdown and concurrent transport measurements in multiwall carbon nanotubes," *Phys. Rev. Lett.*, vol. 94, no. 23, Jun. 2005, Art. no. 236802. [Online]. Available: http://link.aps.org/doi/10.1103/PhysRevLett.94.236802
[34] K. Ghosh, C. C. Yap, B. K. Tay, and C. S. Tan, "Integration of CNT in TSV ($\leq 5\mu m$) for 3D IC application and its process challenges," in *Proc. IEEE Int. 3D Syst. Integr. Conf.*, San Francisco, CA, USA, Oct. 2013, pp. 1–4.
[35] M. Fujii *et al.*, "Measuring the thermal conductivity of a single carbon nanotube," *Phys. Rev. Lett.*, vol. 95, Aug. 2005, Art. no. 065502. [Online]. Available: https://link.aps.org/doi/10.1103/PhysRevLett.95.065502
[36] P. M. Ajayan *et al.*, "Opening carbon nanotubes with oxygen and implications for filling," *Nature*, vol. 362, no. 6420, pp. 522–525, Apr. 1993, doi: 10.1038/362522a0.

Abhishek Mishra, photograph and biography not available at the time of publication.

Harald Gossner, photograph and biography not available at the time of publication.

Mayank Shrivastava, photograph and biography not available at the time of publication.